FUDMA Journal of Sciences (FJS)
ISSN online: 2616-1370
ISSN print: 2645 - 2944
Vol. 7 No. 3, June (Special Issue), 2023, pp 110 - 121
DOI: https://doi.org/10.33003/fjs-2023-0703-1154

MOTION AROUND THE EQUILIBRIUM POINTS IN THE PHOTOGRAVITATIONAL R4BP UNDER THE EFFECT OF CIRCUMSTELLAR BELT

[*1]Aguda Ekele Vincent and [2]Joel John Taura

[1]Department of Mathematics, School of Basic Sciences, Nigeria Maritime University, Okerenkoko, Delta State, Nigeria
[2]Department of Mathematics and Statistics, Federal University of Kashere, Gombe, Gombe State, Nigeria

*Corresponding authors' email: vincentekele@yahoo.com

ABSTRACT

In the present work, we study numerically the motion of an infinitesimal fourth body near the equilibrium points (EPs) of the photogravitational restricted four-body problem (Lagrangian configuration) under the effect of circumstellar belt. We consider the case where three the bodies of masses m_1, m_2 and m_3 (primaries) are sources of radiation as well as enclosed by a circumstellar belt and two of the primaries, m_2 and m_3, have equal masses ($m_2 = m_3 = \mu$) and equal radiation factors ($q_2 = q_3$) while the dominant primary body m_1 is of mass $1 - 2\mu$. Firstly, these equilibria are determined and then the influence of the system parameters on their positions and stability is performed. In addition, the numerical exploration is performed using the Ross 104-Ross775a-Ross775b stellar system to compute the locations of the equilibria and the eigenvalues of the characteristic equation. For this system where the value of the mass parameter is beyond Routh's value, we observe that they may be ten (four collinear and six non-collinear) or eight (two collinear and six non-collinear) EPs depending on the mass of the circumstellar belt. The linear stability of each equilibrium point is also studied and it is found that in the case where ten equilibria exist, the new collinear point, L_{n1} is always linearly stable while the other nine equilibria are always linearly unstable. In the case where eight equilibria exist, all of them are always linearly unstable. The zero velocity surfaces for the stellar system are drawn and regions of motion are analyzed for increasing values of the mass belt.

Keywords: Restricted Four-body problem, Radiation pressure, Circumstellar belt, Equilibrium points, Stability, Zero velocity surfaces

INTRODUCTION

The equilibrium points solutions, their parametric variation and their stability among other dynamical aspects of few-body celestial systems have always been an attractive and important field of research due to the discovery of a great amount of extrasolar planetary systems. The circular restricted three-body problem (henceforth CR3BP) is one of the most attractive and important problems of study in space dynamics as well as in dynamical Astronomy and in its different modifications, has had extensive astronomical applications in several scientific fields, including among others; celestial mechanics, galactic dynamics, lunar and chaos theories (for details see Szebehely, 1967; Murray and Dermott, 1999; Musielak and Quarles, 2017). In this model, two finite bodies, known as primaries, rotate in circular orbits around their common center of mass, while the third infinitesimal body moves under the gravitational attraction of the primaries and does not affect their motion. In the gravitational restricted three-body problem (R3BP), Lagrange, in 1772 showed that there exists five libration points. Three of these points denoted by L_1, L_2, and L_3 are called collinear and they lie on the $x-$axis while the other two denoted by L_4 and L_5 are called triangular points and are away from the $x-$axis (Szebehely, 1967). The three collinear equilibrium points are generally unstable whereas the triangular points are stable for the mass ratio $0 < \mu \leq 0.03852\ldots$ Tyokyaa and Atsue (2020) studied the locations and linear stability of equilibrium points in the CR3BP under radiation and oblatenes of the bigger primary.

The restricted four-body problem (R4BP) is an extension of the R3BP and a natural generalization of it. It deals with the motion of a body of infinitesimal (test particle) mass under the simultaneous gravitational attraction of three massive bodies (primaries) moving in circular periodic orbits around their center of mass fixed at the origin of the coordinate system. The infinitesimal fourth body does not affect the motion of the three bodies. In the case here considered, the primaries of the problem are located at the apices of an equilateral triangle (Lagrangian configuration). We refer to this as the R4BP. Moulton (1900) built this model and already studied its equilibria. Since then, this very special configuration has often been found to be the center of special scientific interest and many authors have focused on the study of the relative equilibrium solutions and their stability, computation of families of periodic orbits, etc not only for the gravitational case but also for cases that include additional forces other than the gravitational one (i.e., post-Newtonian potentials). Some interesting studies of the problem (gravitational case) appeared in the last few years. In the first, Simo (1978) studied the linear stability of the relative equilibrium solutions in the R4BP. In the second (Alvarez-Ramirez and Vidal, 2009), the authors studied the model problem when the three massive primaries have equal masses. In the third one (Baltagiannis and Papadakis, 2011), the authors studied numerically the equilibrium points (EPs) and their stability under different combinations of mass, namely; all primary bodies with equal masses, two primary bodies with equal masses and all the primary bodies with unequal masses. The results indicate that equilibria and stability depend on the ratios of the masses. During the past, the Lagrange configuration of the R4BP has been investigated to understand the influence and effects of several parameters in realistic celestial systems (see e.g. Schwarz et al. 2009a, 2009b; Ceccaroni and Biggs 2012; Baltagiannis and Papadakis 2013).

Several authors have studied the existence of equilibrium points and their stability in the frame of the R4BP under different perturbing forces, but mainly considering three equal masses or two equal masses for the primary bodies. Without

being exhaustive, a number of articles are available in the literature, which are devoted to the study of the EPs and their properties such as their linear stability on the R4BP in the case where some or all the primaries are radiation sources together with additional terms, such as the Stokes drag and/or oblateness or even some versions such as the restricted problem of 2+2 bodies. Papadouris and Papadakis (2013) studied the existence and linear stability of the EPs on the plane, as well as out of the orbital plane in the framework of R4BP with the assumption that the first primary body is a radiation source when the masses of the three primary bodies or the masses of two of them are equal. In the planar motion of the problem where the two small primary bodies have equal masses, it was observed that the problem admits 2 collinear and 6 or 4 noncollinear EPs depend on the radiation coefficient of the dominant primary body. They have shown that the radiation pressure has significant effects on the topology of the zero velocity curves. Soon after, Singh and Vincent (2015, 2016), Ansari (2016), Osorio-Vergas et al. (2020), Suraj et al. (2020) investigated this configuration including radiation of the primaries. Singh and Omale (2019) studied the combined effect of Stokes drag, oblateness and radiation pressure on the existence and stability of EPs in the R4BP. Vincent et al. (2019) studied the existence, location and stability of EPs of the model problem when all the primaries are radiation sources together with Stokes drag effect. It was observed that in the presence of P–R drag effect, the collinear EPs of the problem cease to exist numerically and of course analytically.

Studies of planetary and stellar systems have revealed disc of dust particles which are regarded as young analogues of the Kuiper Belt in the Solar System (Greaves et al., 1998). These discs play important roles in the origin of planets' orbital elements if they are massive enough. The importance of the problem in astronomy has been addressed by Jiang and Yeh (2004, 2006) where it was shown that the presence of disc resulted to additional equilibria of the system. Many scientists took into account the gravitational potential from the belt/disc under various assumptions in R3BP and found that these perturbations exhibit significant changes in the equilibrium position and stability (see e.g., Kishor and Kushvah, 2013; Singh and Taura, 2013; Jiang and Yeh, 2014; Vincent et al., 2022; Vincent and Kalantonis, 2022). Taura and Leke (2022) derived the equations of motion of the CR3BP when the masses of the primaries vary and surrounded by a belt. Furthermore, extensions to more realistic problems in stellar or solar dynamics appeared in some previous works on the R4BP by considering gravitational potential from the belt/disc with additional terms, such as the radiation pressure and Manev potential (Singh and Omale, 2020 and Mahato et al., 2021).

In this study, the inclusion of radiation pressure and gravitational potential from the belt in the R4BP, allow us to model in a more realistic way the dynamics of an infinitesimal particle. In this premise, stellar system Ross 104-Ross775a-Ross775b provides suitable astrophysical model for this problem. In extending the research work by Singh and Vincent (2015, 2016), we aim to study the motion of an infinitesimal body near the equilibrium points of the R4BP when the primaries are modeled as radiation sources with the three stars enclosed by a disc. New equilibrium points, zero-velocity surfaces and allowed regions of motion make a qualitative difference to the dynamical features of the model.

Mathematical formulation and equations of motion

We consider the motion of an infinitesimal particle, say m under the gravitational attraction of three primary bodies m_1, m_2 and m_3, called primaries. We assume that the three primaries can be radiating sources and that primaries m_2 and m_3 have the same mass $m_2 = m_3 = \mu$ and the same radiation factor $q_2 = q_3$. We assume that the primaries are in an equilateral triangle configuration. Specifically, bodies m_2 and m_3 have the horizontal x -axis as symmetric axis such that the body m_1 lies on the negative x -axis at the origin of time. The mutual distances of the three primaries remain unchanged with respect to time. The motion of the system is referred to axes rotating with uniform angular velocity. Their motion consists of circular orbits around their center of gravity. We choose the units of distance, mass and time in such a way that the gravitational constant $G = 1$. Hence, the coordinates of the primaries m_1, m_2, m_3 in the synodic frame (coplanar primaries) are, $(-\mu\sqrt{3}, 0)$, $(\frac{\sqrt{3}}{2}(1-2\mu), -\frac{1}{2})$, and $(\frac{\sqrt{3}}{2}(1-2\mu), \frac{1}{2})$, respectively, and $0 < \mu < \frac{1}{3}$, with μ the so-called mass-ratio parameter.

The equations of motion of the photogravitational restricted four-body problem are written as Singh and Vincent (2015, 2016)

$$\ddot{x} - 2\dot{y} = \Omega_x, \qquad \ddot{y} + 2\dot{x} = \Omega_y, \tag{1}$$

where the potential function, Ω may be written as

$$\Omega = \frac{(x^2+y^2)}{2} + \frac{(1-2\mu)q_1}{r_1} + \frac{\mu q_2}{r_2} + \frac{\mu q_2}{r_3} \tag{2}$$

where

$$r_1 = \sqrt{(x+\sqrt{3}\mu)^2 + y^2},$$
$$r_2 = \sqrt{(x-\frac{\sqrt{3}}{2}(1-2\mu))^2 + (y+\frac{1}{2})^2}, \tag{3}$$
$$r_3 = \sqrt{(x-\frac{\sqrt{3}}{2}(1-2\mu))^2 + (y-\frac{1}{2})^2}, q_2 = q_3.$$

r_1, r_2 and r_3 are the distances of the test particle from the three primaries m_1, m_2 and m_3, respectively, $q_1, q_2, q_3 (q_i \leq 1, i = 1,2,3)$ are the radiation pressure of the first, second and third primary, respectively, while the dot is the differentiation w.r.t time t.

Let us recall that according to Miyamoto and Nagai (1975), the gravitational potential from the disc is given by

$$V(r,z) = -\frac{M_b}{\sqrt{r^2+(a+(\sqrt{z^2+b^2})^2}}, \tag{4}$$

where $M_b (M_b << 1)$ stands for the mass of the disc, r is the radial distance of the dust particle so that $r^2 = x^2 + y^2$, a and b are the flatness and core parameters, respectively. Restricting to coplanar primaries, equation (4) becomes

$$V(r) = -\frac{M_b}{\sqrt{r^2+T^2}}, \tag{5}$$

where $T = a + b$ denotes the density profile of the disc taken to the value $T = 0.02$ (Vincent et al., 2022).

Denoting by n the mean motion of the fourth body, from Singh and Omale (2020), Vincent et al. (2022) and Mahato et al. (2022), we have the following expression

$$n^2 = 1 + \frac{2M_b r_c}{(r_c^2+T^2)^{\frac{3}{2}}} \tag{6}$$

with $r_c^2 = 1 - \mu + \mu^2$, the radial distance of the test particle. Therefore, using equations (6) and (5) and following Singh and Omale (2020) and Singh and Vincent (2016), the pertinent equations of motion (1) in the xy -plane are finally written as

$$\ddot{x} - 2n\dot{y} = n^2 x - \frac{(1-2\mu)(x+\sqrt{3}\mu)q_1}{r_1^3} - \frac{q_2(x-\frac{\sqrt{3}}{2}(1-2\mu))\mu}{r_2^3} - \frac{q_2(x-\frac{\sqrt{3}}{2}(1-2\mu))\mu}{r_3^3} - \frac{M_b x}{(r^2+T^2)^{\frac{3}{2}}}, \tag{7}$$

$$\ddot{y}+2n\dot{x}=n^2 y-\frac{(1-2\mu)yq_1}{r_1^3}-\frac{q_2(y+\frac{1}{2})\mu}{r_2^3}-\frac{q_2(y-\frac{1}{2})\mu}{r_3^3}-\frac{M_b y}{(r^2+T^2)^{\frac{3}{2}}},$$

where the potential function due to the combined effect of radiation pressure and circumstellar belt becomes

$\Omega=\frac{n^2(x^2+y^2)}{2}+\frac{(1-2\mu)q_1}{r_1}+\frac{\mu q_2}{r_2}+\frac{\mu q_3}{r_3}+\frac{M_b}{(r^2+T^2)^{\frac{1}{2}}}$

Equations of motion admits the energy (Jacobi) integral ($C$is the Jacobi constant)

$C+(\dot{x}^2+\dot{y}^2)=2\Omega$ (8)

Linear stability of the equilateral triangle configuration

In the photogravitational R4BP, the necessary condition for the stability of the Lagrange central configuration is described by the inequality (Papadouris and Papadakis, 2013):

$$\frac{q_1m_1q_2m_2+q_2m_2q_3m_3+q_1m_1q_3m_3}{(q_1m_1+q_2m_2+q_3m_3)^2}<\frac{1}{27}, \quad (9)$$

where $q_1, q_2$and $q_3$are the corresponding radiation factors of the primaries. The gravitational case, i.e. $q_1=q_2=q_3=1$, was first studied by Gascheau (1843). In the photogravitational R4BP where one or all the three primary bodies radiate, there are combinations of the system parameters where lead to the equilateral triangle configuration to be linearly stable (Papadouris and Papadakis 2013, Singh and Vincent 2016, Vincent et al. 2019). For this reason, we will adopt sets of (m_i, q_i, M_b) which satisfy the condition (9).

Existence and position of equilibrium points

The equilibrium (Lagrangian) points are those points at which the velocities $\dot{x},\dot{y}$ and accelerations $\ddot{x},\ddot{y}$ of the fourth infinitesimal particle are zero, so that $\dot{x}=\dot{y}=\ddot{x}=\ddot{y}=0$. Invoking these conditions in equations (7), we get,

$$n^2x-\frac{(1-2\mu)(x+\sqrt{3}\mu)q_1}{r_1^3}-\frac{q_2(x-\frac{\sqrt{3}}{2}(1-2\mu))\mu}{r_2^3}-\frac{q_2(x-\frac{\sqrt{3}}{2}(1-2\mu))\mu}{r_3^3}-\frac{M_b x}{(r^2+T^2)^{\frac{3}{2}}}=0, \quad (10)$$

and

$$n^2y-\frac{(1-2\mu)yq_1}{r_1^3}-\frac{q_2(y+\frac{1}{2})\mu}{r_2^3}-\frac{q_2(y-\frac{1}{2})\mu}{r_3^3}-\frac{M_b y}{(r^2+T^2)^{\frac{3}{2}}}=0 \quad (11)$$

It is well-known that in the gravitational R4BP (Lagrangian configuration) where the two small primary bodies have the same mass there are two kinds of equilibria or solution (as in the R3BP) depending on whether $y=0$ or $y\neq 0$. A complete discussion of the gravitational case of the problem can be found in Baltagiannis and Papadakis (2011). It is important to stress that in the case where $M_b=0$and $q_2=q_3=1$, that is the photogravitational version of the R4BP, has been studied in full detail by Papadouris and Papadakis (2013) where, for $q_1\in(0,1]$, the authors examined the existence, location and linear stability of the EPs.

In Fig. 1 we illustrate the eight EPs, two collinear equilibrium points $L_{1,2}$ (on the x -axis) and six noncollinear $L_i, i=3,\ldots,8$ (out of the x -axis) ones of the model problem, which we have found by solving numerically the equations (10) and (11). So, for$\mu=0.006, q_1=0.95, q_2=0.98, M_b=0.03$and $T=0.02$ (Fig. 1a), is easily seen that the problem admits eight EPs. It is worth mentioning that the equilibrium points in the xy -plane are given by mutual intersections of both curves marked by green dots while the centers of the primary bodies, $m_i, i=1,2,3$are denoted by blue dots. More so, the intersection points of these curves are the coordinates (x_0, y_0) of the equilibria by means of an iterative process and that the couples $L_{3,5}, L_{4,6}$and $L_{7,8}$are symmetric w.r.t the x -axis. In Fig. 1b we give the position diagram of Papadouris and Papadakis (2013) when $\mu=0.005, q_1=0.65, q_2=q_3=1$and $M_b=0$, which was reproduced here for comparison and for checking purposes. For this particular case, the numerical solution shown in Fig. 1b agrees with the result presented in Papadouris and Papadakis (2013, see Fig. 7 of that paper).

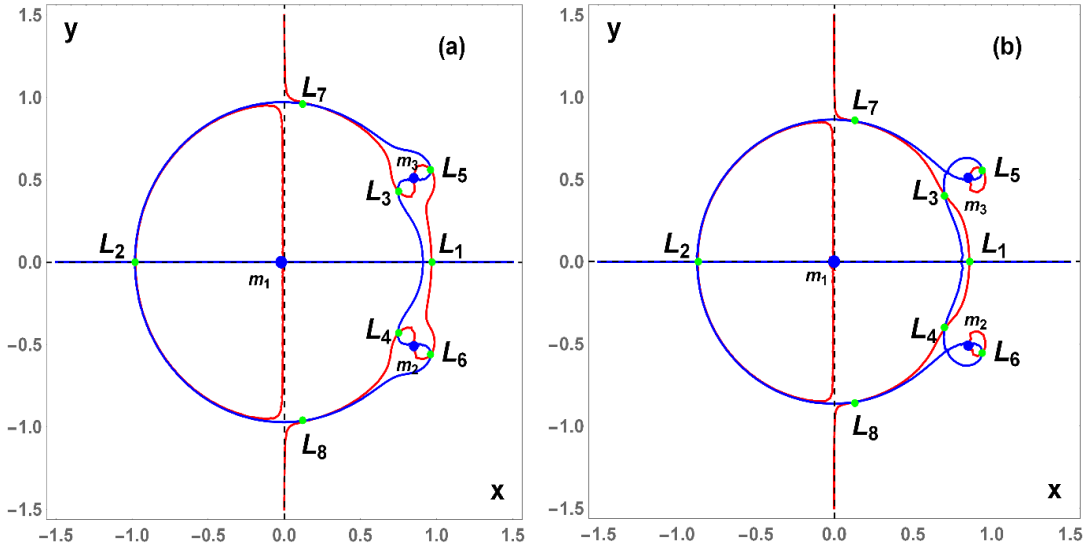

Figure 1: (Color online) The positions (green dots) of the eight equilibrium points$L_i, i = 1,\ldots,8$ when: **(a)** $\mu = 0.006$, $q_1 = 0.95$, $q_2 = 0.98$. $M_b = 0.03$ and $T = 0.02$, **(b)** $\mu = 0.005$, $q_1 = 0.65$, $q_2 = q_3 = 1$ and $M_b = 0$. Blue points indicate the position of the three primary bodies, $m_i, i = 1,2,3$.

Next, the locations of the equilibrium points of the test particle for circumstellar belt variation, $M_b \in [0,0.12]$ when the radiation parameters q_1 and q_2 vary in the interval $q_i \in (0,1]$ shall be discussed. In this case, we consider sets of variation parameters that satisfy condition (9).

To investigate the effect of the radiation pressure of the first primary on the locations of the equilibrium points we set for $\mu = 0.006, q_2 = 0.9, M_b = 0.05$ and $T = 0.02$ with the variation of q_1. The coordinates of the numerically determined equilibrium points are shown in Table 1 for different values of the q_1. We observe that with the increase of q_1 (1to 0.70) for fixed μ, q_2, M_b and T, the coordinates of the eight equilibrium points increase upward or decrease downward. That is, both x -coordinates of L_1 and L_2 decrease while both the x and y coordinates of points L_3, L_5 and L_7 decrease. Fig. 2 is a plot of the locations of the equilibrium points when q_1 varies for fixed values of the chosen parameters model. We observe that with the increase of q_1, the locations of points L_5 and L_6 tend to the primaries m_3 and m_2, correspondingly whereas the locations of all the equilibria move close to the position of the primary body m_1. As we see, the numerical results of the equilibrium positions in Table 1 is similar to the corresponding results presented in Fig. 1.

Table 1: The locations of the equilibrium points $L_i, i = 1,\ldots,8$ as a function of q_1 for $\mu = 0.006, q_2 = 0.9, M_b = 0.05$ and $T = 0.02$

L_i	$q_1 = 1$	$q_1 = 0.85$	$q_1 = 0.70$
$L_1(x,y)$	(0.977043, 0)	(0.926891, 0)	(0.870646, 0)
$L_2(x,y)$	(−0.988149, 0)	(−0.939046, 0)	(−0.884127, 0)
$L_{3,4}(x,\pm y)$	(0.752608, ±0.440456)	(0.733892, ±0.429518)	(0.707169, ±0.413699)
$L_{5,6}(x,\pm y)$	(0.957651, ±0.559552)	(0.947551, ±0.553516)	(0.939267, ±0.548605)
$L_{7,8}(x,\pm y)$	(0.259063, ±0.945657)	(0.220535, ±0.904982)	(0.181070, ±0.857736)

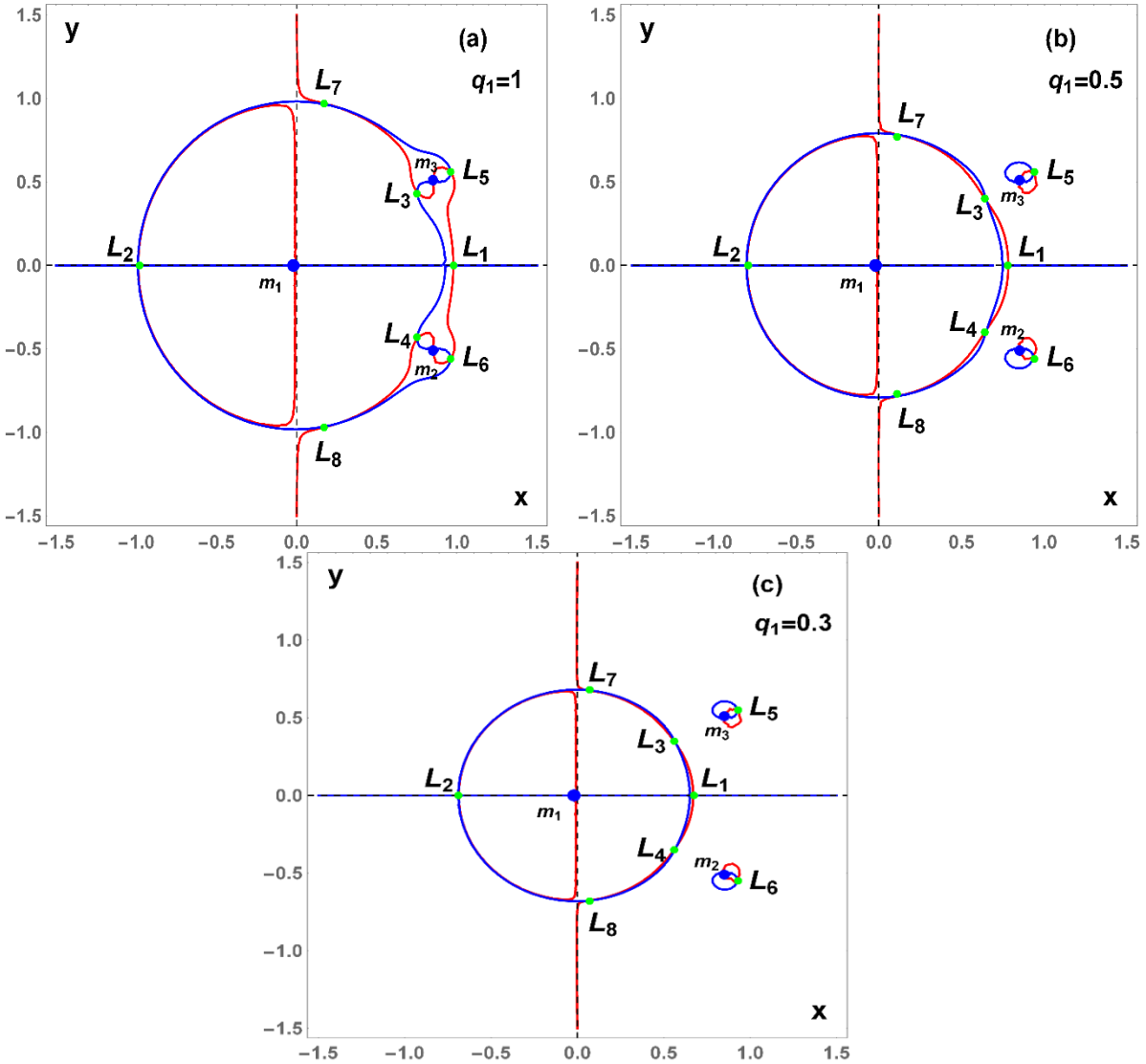

Figure 2: The locations of the eight equilibrium points $L_i, i = 1,\ldots,8$ (green dots) for $\mu = 0.006, q_2 = 0.9, M_b = 0.05andT = 0.02$ when only the radiation pressure of the first primary varies, i.e., panels: **(a)** for $q_1 = 1$, **(b)** $q_1 = 0.5$, and **(c)** $q_1 = 0.3$. The centers of the primary bodies, $m_i, i = 1,2,3$are denoted by blue dots.

The influence of the common radiation factor q_2 of the primary bodies m_2 and m_3 on the locations of the eight equilibrium points is presented in Table 2 for fixed values of the chosen parameters. Here, it is observed that with the increase of radiation factor q_2 (1 to 0.70) for fixed values of μ, q_1, M_b and T, x -coordinates of both L_1 and L_2 decrease; both x and y coordinates of L_3 increase; both the x and $y$coordinates ofL_5 decrease while the x and y coordinates of L_7 increase and decrease, respectively. In Fig. 3, we have presented numerically the locations of the eight equilibrium points for various values of the parameter q_2 when the values of the remaining parameters μ, q_1, M_b and T are fixed. We observe that for increasing values of the radiation factor of both primary bodies m_2 and m_3, locations of points$L_1$and L_2 both approach the dominant primary body m_1 ; L_3, L_5, L_7tend to the primary body $m_3$while at the same time L_4, L_6, L_8tend to m_2. These effects can be easily seen in Table 2.

Table 2. The locations of the equilibrium points $L_i, i = 1,\ldots,8$as a function of $q_2$for $\mu = 0.006, q_1 = 0.9, M_b = 0.05andT = 0.02$

L_i	$q_2 = 1$	$q_2 = 0.85$	$q_2 = 0.70$
$L_1(x, y)$	(0.944465, 0)	(0.944082, 0)	(0.943703, 0)
$L_2(x, y)$	(−0.956081, 0)	(−0.955933, 0)	(−0.955785, 0)
$L_{3,4}(x, \pm y)$	(0.737715, ±0.431508)	(0.742551, ±0.434721)	(0.748022, ±0.438333)
$L_{5,6}(x, \pm y)$	(0.954697, ±0.557579)	(0.948596, ±0.554235)	(0.941786, ±0.550468)
$L_{7,8}(x, \pm y)$	(0.196452, ±0.928198)	(0.252527, ±0.913934)	(0.312452, ±0.894562)

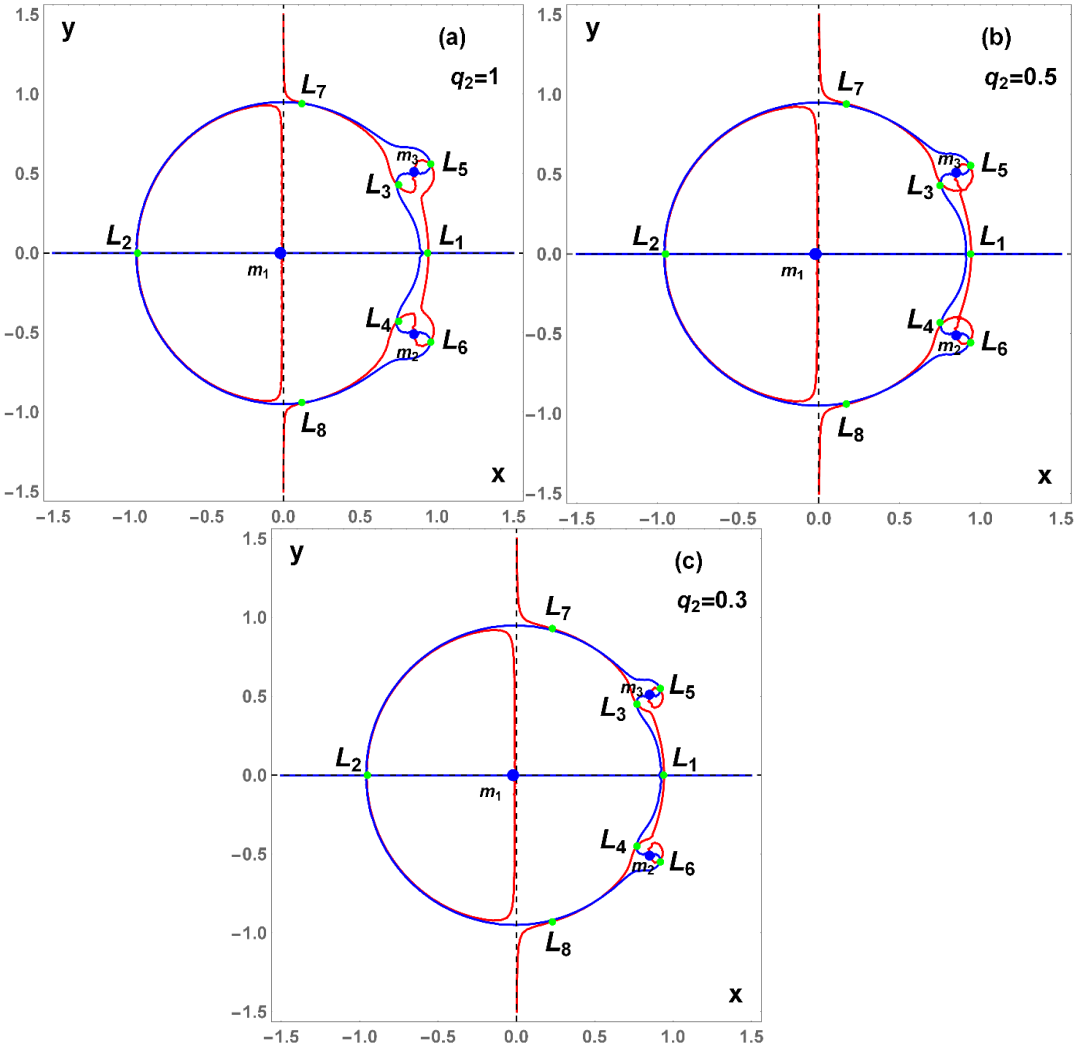

Figure 3: The locations of the eight equilibrium points $L_i, i = 1,\ldots,8$ (green dots) for $\mu = 0.006, q_1 = 0.9, M_b = 0.05andT = 0.02$ when only the common radiation pressure of the primary bodies $m_2$and $m_3$radiates, i.e., panels: **(a)** for $q_2 = 1$, **(b)** $q_2 = 0.5$, and **(c)** $q_2 = 0.3$. The centers of the primary bodies, $m_i, i = 1,2,3$are denoted by blue dots.

Similarly, for the investigation of the effect of the mass of disc $M_b$on the locations of the EPs we set for $\mu = 0.006, q_1 = 0.85, q_2 = 0.95$ and $T = 0.02$ while M_b varies. The coordinates of the corresponding EPs are shown in Table 3 for various values of mass of the disc M_b. With the increase of M_b from 0 to 0.05, x -coordinates of both L_1 and L_2 decrease; both the$x$ and $y$coordinates of L_3 and L_5decrease while the x and y coordinates of L_7 increase and decrease, respectively. In Fig. 4 we plot the respective locations of the equilibrium points when the mass of disc varies for fixed values of the parameters. As we observe, the variational trend of the equilibrium locations in Fig. 4 is similar to the corresponding scenario presented in Table 3. It can be seen that locations of pointsL_1,L_2,$L_3$and L_4all tend to the dominant primary body m_1 , L_5 and L_7 tend to the primary body m_3 whereas points$L_6$and L_8tend to m_2. These effects can be easily seen in Table 3.

Table 3: The locations of the equilibrium points $L_i, i = 1,\ldots,8$as a function of $M_b$for $\mu = 0.006, q_1 = 0.85, q_2 = 0.95andT = 0.02$

L_i	$M_b = 0$	$M_b = 0.03$	$M_b = 0.05$
$L_1(x, y)$	(0.939005, 0)	(0.931553, 0)	(0.926995, 0)
$L_2(x, y)$	(−0.95144, 0)	(−0.943792, 0)	(−0.939096, 0)
$L_{3,4}(x, \pm y)$	(0.734128, ±0.429463)	(0.733034, ±0.428847)	(0.732322, ±0.428446)
$L_{5,6}(x, \pm y)$	(0.955369, ±0.557959)	(0.951767, ±0.555891)	(0.949568, ±0.554627)
$L_{7,8}(x, \pm y)$	(0.196536, ±0.922992)	(0.199799, ±0.914665)	(0.201813, ±0.909542)

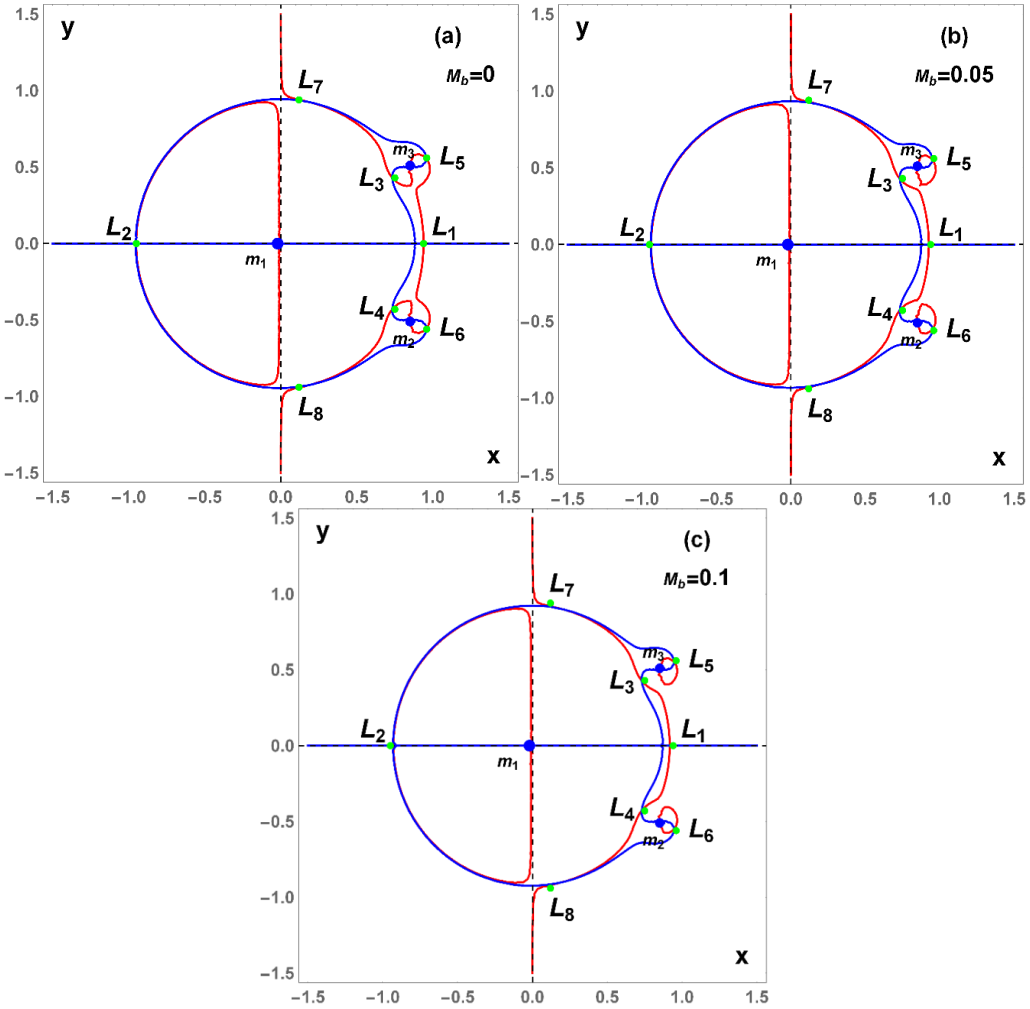

Figure 4: The locations of the eight equilibrium points $L_i, i = 1,\ldots,8$ (green dots) for $\mu = 0.006, q_1 = 0.85, q_2 = 0.95andT = 0.02$ when the mass of the disc varies, i.e., panels: **(a)** for $M_b = 0$, **(b)** $M_b = 0.03$, and **(c)** $M_b = 0.1$. The centers of the primary bodies, $m_i, i = 1,2,3$are denoted by blue dots

It is obvious from Tables 1—3 and Figures 2—4 that the system parameters (q_1, q_2, M_b) effect the locations of the equilibrium points significantly. We also observed from the aforementioned discussion that the locations of the equilibrium points vary in a relatively small range with $M_b$compared to the radiation pressure$q_2$and to q_1.

Stability of the equilibrium points

The stability of the equilibrium points can be determined by linearizing the equations of motion. In doing this, we let the position of an equilibrium point be denoted by (x_0, y_0) and consider a small displacement (ξ, η) from the point such that

$$x - x_0 = \xi, y - y_0 = \eta. \quad (12)$$

Substituting equations (12) into equations (7), we obtain the variational form of the equations of motion as

$$\ddot{\xi} - 2n\dot{\eta} = \xi(\Omega^0_{xx}) + \eta(\Omega^0_{xy}), \quad (13)$$

$$\ddot{\eta} + 2n\dot{\xi} = \xi(\Omega^0_{yx}) + \eta(\Omega^0_{yy}) \quad (14)$$

where only linear terms in $\xi$and η have been taken.

Accordingly, the characteristic equation corresponding to equations (13) and (14) is given as

$$\lambda^4 + (4n^2 - \Omega^{(0)}_{xx} - \Omega^{(0)}_{yy})\lambda^2 + \Omega^{(0)}_{xx}\Omega^{(0)}_{yy} - [\Omega^{(0)}_{xy}]^2 = 0 \quad 15)$$

where the second partial derivatives are denoted by subscripts while the superscript (0) means evaluation at the coordinates (x_0, y_0) of the EPs with

$$\Omega^{(0)}_{xx} = n^2 - \frac{(1-2\mu)q_1}{r_{10}^3} + \frac{3q_1(1-2\mu)(x_0+\sqrt{3}\mu)^2}{r_{10}^5} - \frac{\mu q_2}{r_{20}^3} + \frac{3\mu q_2(x_0 - \frac{\sqrt{3}}{2}(1-2\mu))^2}{r_{20}^5} - \frac{\mu q_2}{r_{30}^3} +$$
$$+ \frac{3\mu q_2(x_0 - \frac{\sqrt{3}}{2}(1-2\mu))^2}{r_{30}^5} - \frac{M_b}{(T^2+r^2)^{\frac{3}{2}}} + \frac{3M_b x_0^2}{(T^2+r^2)^{\frac{5}{2}}}, \quad (16)$$

$$\Omega^{(0)}_{yy} = n^2 - \frac{(1-2\mu)q_1}{r_{10}^3} + \frac{3q_1 y_0^2(1-2\mu)}{r_{10}^5} - \frac{\mu q_2}{r_{20}^3} + \frac{3\mu q_2(y_0+\frac{1}{2})^2}{r_{20}^5} - \frac{\mu q_2}{r_{30}^3} + \frac{3\mu q_2(y_0-\frac{1}{2})^2}{r_{30}^5} - \frac{M_b}{(T^2+r^2)^{\frac{3}{2}}} + \frac{3M_b y_0^2}{(T^2+r^2)^{\frac{5}{2}}}, \quad (17)$$

$$\Omega^{(0)}_{xy} = \Omega^{(0)}_{yx} = \frac{3y_0 q_1(1-2\mu)(x_0+\sqrt{3}\mu)}{r_{10}^5} + \frac{3\mu q_2(y_0+\frac{1}{2})(x_0-\frac{\sqrt{3}}{2}(1-2\mu))}{r_{20}^5} + \frac{3\mu q_2(y_0-\frac{1}{2})(x_0-\frac{\sqrt{3}}{2}(1-2\mu))}{r_{30}^5} + \frac{3M_b x_0 y_0}{(T^2+r^2)^{\frac{5}{2}}}, \quad (18)$$

and

$$r_{10}=\sqrt{(x_0+\sqrt{3}\mu)^2+{y_0}^2},\qquad r_{20}=\sqrt{(x-\frac{\sqrt{3}}{2}(1-2\mu))^2+(y+\frac{1}{2})^2},$$
$$r_{3_0}=\sqrt{(x_0-\frac{\sqrt{3}}{2}(1-2\mu))^2+(y_0-\frac{1}{2})^2},\qquad r_0=\sqrt{{x_0}^2+{y_0}^2} \tag{19}$$

Solving equation (15), we have,

$$\lambda_{1,2}=\pm\frac{1}{\sqrt{2}}\left(-b+\sqrt{b^2-4c}\right)^{\frac{1}{2}},\quad \lambda_{3,4}=\pm\frac{1}{\sqrt{2}}\left(-b-\sqrt{b^2-4c}\right)^{\frac{1}{2}}, \tag{20}$$

where, $b=4n^2-\Omega_{xx}^{(0)}-\Omega_{yy}^{(0)}$ and $c=\Omega_{xx}^{(0)}\Omega_{yy}^{(0)}-(\Omega_{xy}^{(0)})^2$.

Here, discriminant, $\Delta=b^2-4c$ (21)

Equations (20) are the eigenvalues of the characteristics equation (15).

The stability or instability of motion around an equilibrium point can be accomplished through the numerical computation of the characteristic roots of equation (15).

Stability of the collinear equilibrium points

For the collinear equilibrium points $(x_0,0)$, condition $y=0$and the quantities are

$$\Omega_{xx}^{(0)}=n^2-\frac{(1-2\mu)q_1}{r_{*10}^3}+\frac{3q_1(1-2\mu)(x_0+\sqrt{3}\mu)^2}{r_{*10}^5}-\frac{\mu q_2}{r_{*20}^3}+\frac{3\mu q_2(x_0-\frac{\sqrt{3}}{2}(1-2\mu))^2}{r_{*20}^5}-\frac{\mu q_2}{r_{*30}^3}+$$
$$+\frac{3\mu q_2(x_0-\frac{\sqrt{3}}{2}(1-2\mu))^2}{r_{*30}^5}-\frac{M_b}{(T^2+r^2)^{\frac{3}{2}}}+\frac{3M_bx_0^2}{(T^2+r^2)^{\frac{5}{2}}}, \tag{22}$$
$$\Omega_{yy}^{(0)}=n^2-\frac{(1-2\mu)q_1}{r_{*10}^3}-\frac{\mu q_2}{r_{*20}^3}+\frac{3\mu q_2}{4r_{*20}^5}-\frac{\mu q_2}{r_{*30}^3}+\frac{3\mu q_2}{4r_{*30}^5}-\frac{M_b}{(T^2+r^2)^{\frac{3}{2}}}, \tag{23}$$
$$\Omega_{xy}^{(0)}=\Omega_{yx}^{(0)}=0 \tag{24}$$

with $r_{*10}=\left|x_0+\sqrt{3}\mu\right|,\quad r_{*20}=r_{*30}=\sqrt{(x_0-\frac{\sqrt{3}}{2}(1-2\mu))^2+\frac{1}{4}}$

Let us note that linear stability condition will be accomplished if

$$b^2-4c>0,\quad b>0,\quad c>0. \tag{25}$$

Stability of the non-collinear equilibrium points.

The stability of the noncollinear EPs of the problem may be approximated by equations (15) —(19). An equilibrium point (x_0,y_0) is said to be stable if equation (15), evaluated at the equilibrium, has pure imaginary roots or complex roots with negative real parts; otherwise, it is unstable. Due to the symmetry of the model problem, we conclude that the stability of a negative equilibrium is the same that the stability of its symmetric positive equilibrium. For this reason, it will be sufficient to study the stability of the positive equilibria. It is expedient to make stability analysis of the obtained equilibrium solutions in the domain restricted by equation (9).

As a particular example we compute the characteristic roots $\lambda_{1,2},\lambda_{3,4}$of the equilibrium points $L_i(i=1,\ldots,8)$, which are shown in Table 4 for the values of $\mu=0.006,T=0.02$and relatively extreme values of the mass disc and radiation factors,$M_b=0.08$, $q_1=0.24$and$q_2=0.5$, respectively. It is observed that there are cases in which the eigenvalues are all pure imaginary (equilibrium points $L_1,L_{7,8}$) leading thus to stability while for the equilibrium points $L_2,L_{3,4},L_{5,6}$ we obtain two opposite real roots and two imaginary which means that these points are unstable due to the real roots.

Table 4: The eigenvalues $\lambda_{1,2},\lambda_{3,4}$of equation (15) and the corresponding positions of the equilibrium points $L_i,i=1,\ldots,8$for$M_b=0.08,\mu=0.006,q_1=0.24,q_2=0.5andT=0.02$

L_i	(x_0,y_0)	$\lambda_{1,2}$	$\lambda_{3,4}$	Remark
L_1	(0.641331, 0)	$\pm0.474408i$	$\pm0.94912i$	Stable
L_2	(−0.654644, 0)	±0.186018	$\pm1.08818i$	Unstable
$L_{3,4}$	(0.545991, ±0.329458)	±0.485349	$\pm1.14054i$	Unstable
$L_{5,6}$	(0.904721, ±0.528587)	±5.596970	$\pm4.12410i$	Unstable
$L_{7,8}$	(0.217003, ±0.609500)	$\pm0.294843i$	$\pm1.03291i$	Stable

Numerical Application

In this section, the existence, location and stability of the equilibrium points as discussed numerically and graphically, in the previous sections 3 and 4 are explored numerically for the stellar system: Ross 104-Ross775a-Ross775b for some assumed various values of the mass of the disc. We consider the system because it is of astrophysical interest and its practical applicability to our system model. The values of the data used for the system were borrowed from Vincent et al. (2019). The dominant star, Ross 104 has a mass $0.42M_{Sun}$ and bolometric luminosity 0.020 along with its binary star, Ross 775a and Ross 775b each having equal mass $0.23M_{Sun}$ and bolometric luminosity of 0.20, respectively, which gives a mass ratio μ =0.261363636 that lies above interval where the triangle configuration is linearly stable.

The mass reduction factors are given by the relations: $q_i=1-\frac{AkL}{\alpha\rho M},i=1,2,3,$ (Xuetang and Lizhong 1993) where M, L,

α and ρ are the mass, luminosity, radius and density of the dust grain particle, respectively. Also $A = 2.9838 \times 10^{-5}$ is a constant in the C.G.S system of unit, and κ is the radiation pressure efficiency factor of a star, and it is considered as a unity following Stefan-Boltzmann's law. Now given a test particle with radius $\alpha = 2 \times 10^{-2} cm$ and density $\rho = 1.4 g.cm^{-3}$ (Xuetang and Lizhong, 1993), then$q_{ROSS}104$=$q_1 = 0.9995264$, and $q_{ROSS}775$=$q_2 = q_3 = 0.9913514$. We now proceed to study the influence of mass of the disc on the motion of a test particle using the astrophysical parameters presented above.

In Fig. 5 we present numerically the exact positions of the equilibrium points of the stellar system, for two different values of the mass discM_b. In particular, Fig. 5a depicts the position of the eight equilibrium points (two collinear and six noncollinear) for the case where $M_b = 0.01$. For $M_b = 0.05$we observe in Fig. 5b, that the problem has two more collinear points $L_{ni}, i = 1,2$ located on the negative x -axis between the primary body m_1 and the origin and the problem now has four collinear EPs, making up a total of ten EPs of the problem. In both cases we have fixed the remaining parameters to $\mu = 0.261363636$, $q_1 = 0.9995264$, $q_2 = q_3 = 0.9913514$and $T = 0.02$. From these figures (Fig. 5a, b) we can observe that the mass of belt affects the number of EPs of the problem.

Table 5 shows the location of the eight equilibrium points and the corresponding characteristics roots for the stellar system when $M_b = 0.01$ and $T = 0.02$. Result analysis of Table 5 shows no case in which the roots are pure imaginary. Hence, we conclude that all the EPs are unstable. In Table 6, we compute the location of the ten EPs and the corresponding characteristic roots for the stellar system when $M_b = 0.05$ and $T = 0.02$. In this case, our numerical exploration in the computation of these roots as shown below reveals that the motion of the test body within the neighborhood of each of the equilibria $L_1, L_{n2}, L_2, L_{3(4)}, L_{5(6)}, L_{7(8)}$ is linearly unstable due to the absence of pure imaginary roots or a complex root with a negative real while point L_{n1} is linearly stable due to pure imaginary roots. For the below results we conclude that the circumstellar disc effect on a moving test particle leads to the stability (i.e., out the interval where the Lagrange configuration is linearly stable) of pointL_{n1} arising due to the mass of the disc.

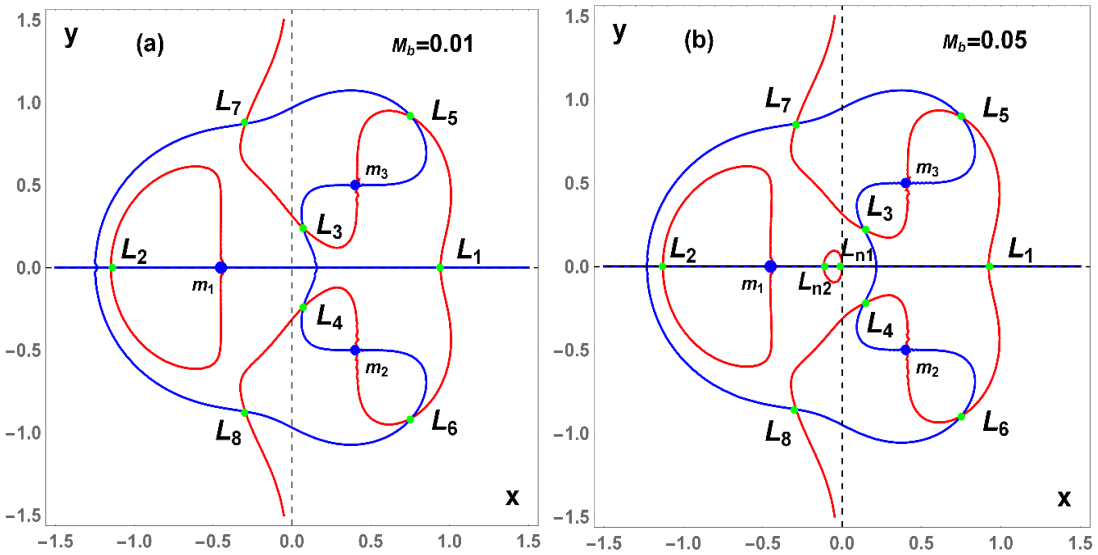

Figure 5 **(a)** Locations of the eight equilibrium points of Ross 104-Ross775a-Ross775b stellar system for fixed values of $M_b = 0.01$and $T = 0.02$, **(b)** Locations of the ten equilibrium points of Ross 104-Ross775a-Ross775b stellar system for fixed values of $M_b = 0.05$and $T = 0.02$. The locations of the primary bodies, $m_i, i = 1,2,3$are denoted by blue dots while green dots indicate the location of the equilibrium points.

Table 5 The eigenvalues $\lambda_{1,2}, \lambda_{3,4}$ of equation (15) and the corresponding locations (x_0, y_0) of the eight equilibria for Ross 104-Ross775a-Ross775b stellar system when $M_b = 0.01$and $T = 0.02$

Point	(x_0, y_0)	$\lambda_{1,2}$	$\lambda_{3,4}$	Remark
L_1	(0.943018, 0)	$-0.861291 \pm 1.00123i$	$0.861291 \pm 1.00123i$	Unstable
L_2	$(-1.14837, 0)$	± 1.08262	$\pm 1.29637i$	Unstable
$L_{3,4}$	$(0.0728597, \pm 0.238108)$	± 3.06217	$\pm 2.13587i$	Unstable
$L_{5,6}$	$(0.761376, \pm 0.909749)$	± 1.36798	$\pm 1.42345i$	Unstable
$L_{7,8}$	$(-0.296565, \pm 0.87182)$	$-0.746164 \pm 0.972082i$	$0.746164 \pm 0.972082i$	Unstable

Table 6: The eigenvalues $\lambda_{1,2}, \lambda_{3,4}$ of equation (15) and the corresponding locations (x_0, y_0) of the ten equilibria for Ross 104-Ross775a-Ross775b stellar system when $M_b = 0.05$and $T = 0.02$

Point	(x_0, y_0)	$\lambda_{1,2}$	$\lambda_{3,4}$	Remark
L_1	(0.922616, 0)	$-0.902507 \pm 1.04984i$	$0.902507 \pm 1.04984i$	Unstable
L_{n1}	$(-0.000247, 0)$	$\pm 77.955i$	$\pm 80.078i$	Stable
L_{n2}	$(-0.115165, 0)$	± 9.143	$\pm 6.59792i$	Unstable
L_2	$(-1.129200, 0)$	± 1.14138	$\pm 1.36139i$	Unstable
$L_{3,4}$	$(0.136703, \pm 0.222941)$	± 3.76263	$\pm 2.62670i$	Unstable

$L_{5,6}$	(0.749644, $\pm$0.896645)	$\pm$1.45194	$\pm 1.50111i$	Unstable
$L_{7,8}$	($-$0.289553, $\pm$0.856112)	$-0.778658 \pm 1.01727i$	$0.778658 \pm 1.01727i$	Unstable

Zero velocity surfaces (zvs) when $M_b = 0$ or $M_b > 0$

We plot in Fig. 6 the zero velocity surface (8) for Ross 104-Ross775a-Ross775b stellar system for various values of $M_b$when: (a) the mass of the disc is absent and (b and c) the mass of the disc varies. From these figures we can observe three main results. The first is a change of the Jacobi constant values which correspond to all equilibrium points with or without circumstellar belt due to which results of zvs show the chaotic behavior. Note the different values of the Jacobi constants C of the panels (b and c) w.r.t panel (a). The second is the emergence, on the side of m_1, the new collinear equilibrium points besides the two gravitational points (see panels (b) and (c)). The third is an enlargement of the "chimneys" which increase the area of the permitted fourth body's motion in the neighborhood of the massive primary body as well in the neighborhood of the other two primaries. The test particle is permitted to move inside the "chimney" and below it. In this case, for a given value of the Jacobi constant *C* and as the mass of the disc increases, the allowed regions of the fourth body motion around the three primaries expand (panel c). This means theoretically that, fourth body can move free around the primaries for bigger and bigger values of the Jacobian constant *C* as the mass of disc parameter increases. It is obvious from these figures that the circumstellar belt under consideration have significant effect where the motion of the test particle is allowed or forbidden in the vicinity of the stellar system, comparing the first frame with the second and third ones.

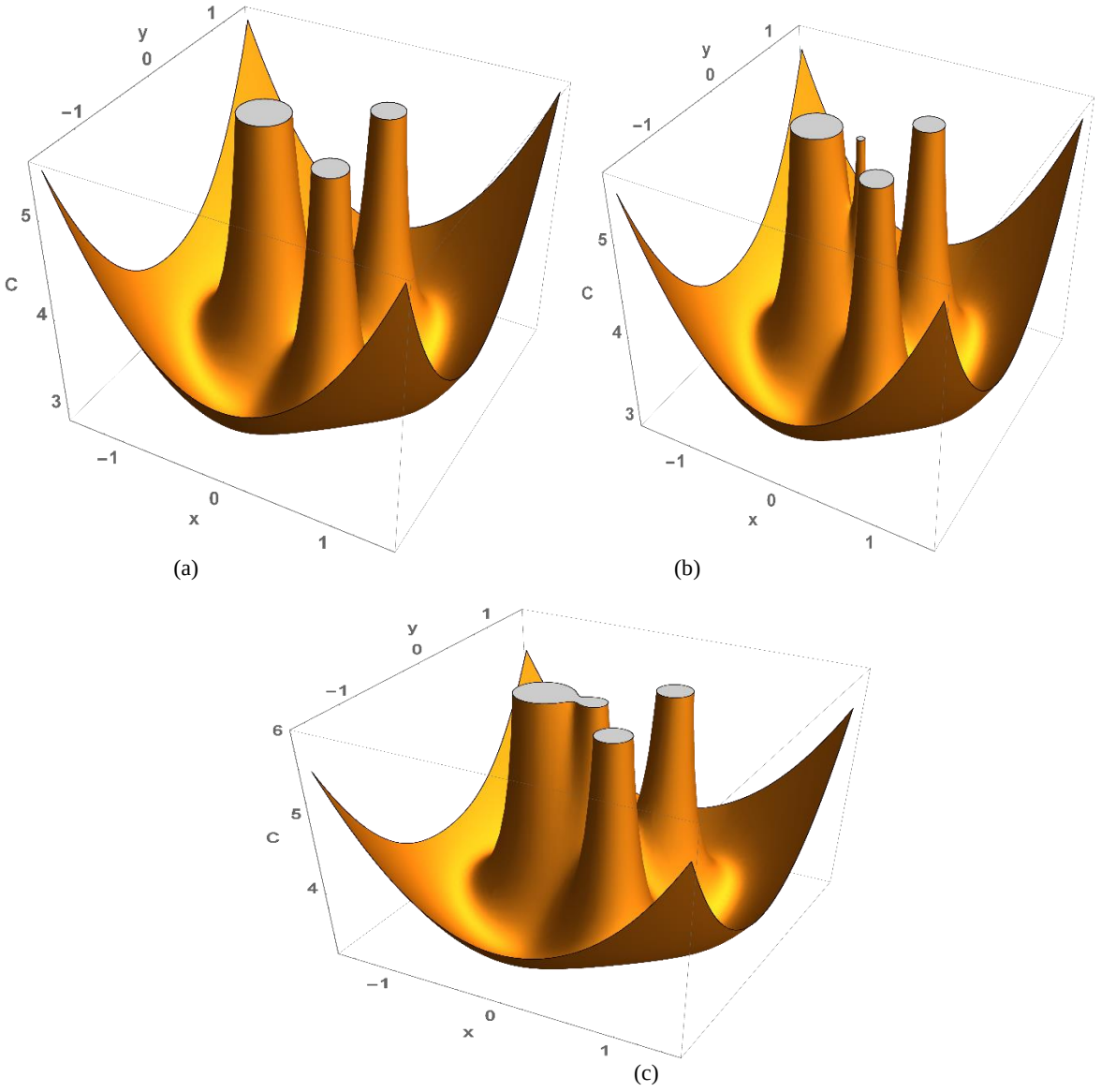

Figure 6: (Colour figure online) Zero velocity surfaces of Ross 104-Ross775a-Ross775b stellar system for (a) $M_b = 0$, (b)$M_b = 0.04$, (c) $M_b = 0.12$. For all cases, the parameter $T = 0.02$ has been used. Motion is allowed inside the chimneys and below it. Note the different scale of *C* in the first and the next frames.

DISCUSSION

In this study we have numerically explored the photogravitational restricted four-body problem under gravitational potential from the belt when three bodies of masses m_1, m_2 and m_3 lie always at the apices of an equilateral triangle (Lagrangian configuration). The fourth body in this system does not affect the motion of the three bodies, and its motion is perturbed by radiation pressure and circumstellar belt from the three primary bodies. In particular, we studied the existence, position and stability of the equilibrium points as the involved parameters vary in the case of two equal masses and two equal radiation factor for the primaries. We found that eight equilibrium points may lie on the plane of motion in a stable Lagrangian configuration of the primaries (see Figs. 1—4 and Tables 1—3). It was observed that the parameters of the model problem not only affect the total number and locations of the equilibrium points but they play remarkable role on their linear stability since it was observed that there are values of these parameters for which the equilibria may be stable. As a particular example, the characteristics roots for the equilibrium points under the combined effect of the involved parameters are calculated numerically and presented in Table 4. It is found that all the equilibria are unstable exceptL_1,L_7 and L_8 which are stable due to the existence of purely imaginary roots.

CONCLUSION

These results have been applied to the stellar system: Ross 104-Ross775a-Ross775b as presented in Figs. 5 and 6 and Tables 5 and 6. It was observed that the total number and distribution of equilibrium points on the plane of motion differ as a result of the mass belt effect. Specifically, it is observed that when the influence of the belt is considered, a pair of collinear points L_{n1}, L_{n2}may appears very near to the origin of the plane for the system, in addition to the two critical points L_1, L_2 , of the gravitational case, making up a total of four collinear points (Fig. 5). More so, the region permitted to motion of the test particle (see Fig. 6) is sensitive to change in the mass of belt for the stellar system. We linearized the equations of motion and computed the characteristic roots for the stellar system. It is observed that the stability state in the case where eight EPs exists are unstable (Table 5), while for the case of ten equilibrium points, all points of equilibrium are always linearly unstable, except equilibrium point L_{n1}, which is stable (see Table 6).
The model of this study can be used to study the behavior of other phenomenon of interest in astronomy, celestial mechanics and astrophysics.

FUNDING ACKNOWLEDGMENT

During this work the first author, Aguda E. Vincent was in receipt of a "Tertiary Education Trust Fund (tetfund, 2021 Intervention)- Nigeria" Institution-Based Research Grant.

REFERENCES

Alvarez-Ramírez, M. and Vidal, C. (2009): Dynamical aspects of an equilateral restricted four-body problem. Math. Probl. Eng. 181360, 1–23

Ansari, A. (2016): The photogravitational circular restricted four-body problem with variable masses. Journal of Engineering and Applied Science 3(2): 30–38.

Baltagiannis, A.N. and Papadakis, K.E. (2011): Equilibrium points and their stability in the restricted four-body problem. Int. J. Bifurc. Chaos 21, 2179–2193

Baltagiannis, A.N. and Papadakis, K.E. (2013): Periodic solutions in the Sun-Jupiter-Trojan Asteroid-Spacecraft system. Planet. Space Sci. 75, 148–157

Ceccaroni, M. and Biggs, J. (2012): Low-thrust propulsion in a coplanar circular restricted four body problem. Celest. Mech. Dyn. Astron. 112, 191–219

Gascheau, G. (1843): Examen d'une classe d'équations différentielles et applications à un cas particulier du problème des trois corps. C. R. Acad. Sci. 16, 393—394

Govind, M.; Pal, A.K.; Alhowaity, S.; Abouelmagd, E.I. and Kushvah, B.S. (2022): Effect of the Planetesimal Belt on the Dynamics of the Restricted Problem of 2 + 2 Bodies. Appl. Sci., 12, 424. https://doi.org/10.3390/app12010424

Greaves, J.S., Holland, W. S., Moriarty-Schieven, G., Jenness, T., Dent, W. R., Zuckerman, B., Mccarthy, C., Webb, R. A., Butner, H. M., Gear, W. K. and Walker, H. J. (1998): A dust ring around Eridani: Analog to the young Solar System, Astrophys. J. 506, 133–137

Jiang, I.G and Yeh, L.C. (2004): The drag-induced resonant capture for Kuiper Belt objects, Mon. Not. R. Astron. Soc. 355, 29–32

Jiang, I.G. and Yeh L. C. (2006): On the Chermnykh-like problem: The equilibrium points, Astrophys. Space Sci. 305, 341–345

Jiang, I. G. and Yeh, L. C. (2014): Galaxies with super massive binary black holes: (I) A possible model for the centers of core galaxies, Astrophys. Space Sci. 349, 881–893.

Kishor, R. and Kushvah, B. S. (2013): Linear stability and resonances in the generalized photogravitational Chermnykh-like problem with a disc, Mon. Not. R. Astron. Soc. 436, 1741–1749

Miyamoto, M. and Nagai, R. (1975); Three-dimensional models for the distribution of mass in galaxies, Publ. Astron. Soc. Jpn. 27, 533–543 (1975).

Moulton, F.R. (1900): On a class of particular solutions of the problem of four bodies. Am. J. Math. 1, 17–29

Murray, C. and Dermott, S. (1999): Solar System Dynamics. Cambridge University Press, Cambridge

Musielak, Z. and Quarles, B. (2017): Three body dynamics and its applications to exoplanets. *In Springer Briefs in Astronomy*, Springer, Cham, Switzerland

Osorio-Vargas, J. E., Dubeibe, F. L. and Gonzalez, G. A. (2020): Orbital dynamics in the photogravitational restricted four-body problem: Lagrange configuration, Physics Letters A 384 126305.

Papadouris, J.P. and Papadakis, K.E. (2013): Equilibrium points in the photogravitational restricted four-body problem. Astrophys. Space Sci. 344, 21–38

Schwarz, R., Süli, À., Dvorac, R. and Pilat-Lohinger, E. (2009a): Stability of Trojan planets in multi-planetary systems. Celest. Mech. Dyn. Astron. 104, 69–84

Schwarz, R., Süli, À. And Dvorac, R. (2009b): Dynamics of possible Trojan planets in binary systems. Mon. Not. R. Astron. Soc. 398, 2085–2090

Simo, C. (1978): Relative equilibrium solutions in the four body problem. Celest. Mech. 18, 165—184

Singh, J. and Vincent, A.E. (2015): Out-of-plane equilibrium points in the photogravitational restricted four-body problem. Astrophys. Space Sci. 359, 38

Singh, J. and Vincent, A.E. (2016): Equilibrium points in the restricted four body problem with radiation pressure. Few-Body Syst. 57, 83–91

Singh, J. and Omale, S.O. (2019): Combined effect of Stokes drag, oblateness and radiation pressure on the existence and stability of equilibrium points in the restricted four-body problem. Astrophys. Space Sci. 364, 6

Singh. J. and Taura, J. J. (2013): Motion in the generalized restricted three-body problem, Astrophys. Space Sci. 343, 95–106

Singh, J., Omale, S.O., Inumoh, L. O. and Ale, F. (2020): Impact of radiation pressure and circumstellar dust on motion of a test particle in Manev's field, Astrodynamics https://doi.org/10.1007/s42064-020-0071-z

Suraj, M. S., Aggarwal, R., Asique, M. C. and Mittal, A. (2020): The effect of radiation pressure on the basins of convergence in the restricted four-body problem, Chaos, Solitons & Fractals 141, 110347.

Szebehely, V. (1967): Theory of Orbits. The Restricted Problem of Three Bodies. Academic Press, New York.
Taura and Leke (2022): Derivation of the dynamical equations of motion of the R3BP with variable masses and disk. *FUDMA Journal of Sciences (FJS*) 6 (4): 125 – 133.

Tyokyaa, K. R. and Atsue, T (2020): Positions and stability of libration points in the radiating and oblating bigger primary of circular restricted three-body problem. *FUDMA Journal of Sciences (FJS*) 4 (2) :523 – 531

Vincent, A. E., Taura, J. J. and Omale, S. O. (2019): Existence and stability of equilibrium points in the photogravitational restricted four- body problem with Stokes drag effect, Astrophysics and Space Science 364 (10)

Vincent, A. E., Perdiou, A. E. and Perdios, E. A. (2022): Existence and stability of equilibrium points in the R3BP with Triaxial-Radiating primaries and an oblate massless body under the effect of the Circumbinary disc. Front. Astron. Space Sci. 9:877459.

Vincent, E.A. and Kalantonis, V.S. (2022): Motion around the equilibrium points in the photogravitational R3BP under the effects of Poynting-Robertson drag, circumbinary belt and triaxial primaries with an oblate infinitesimal body: application on Achird binary system. In: Rassias, Th.M., Pardalos, P. (Eds.), Analysis, Geometry, Nonlinear Optimization and Applications, to be published